THREE-DIMENSIONAL STRUCTURE OF SHEDDING VORTICES BEHIND A V-GUTTER

Takeshi Saito, Naoshi Kuratani, Yuji Ikeda, Tsuyoshi Nakajima

Department of Mechanical Engineering
Kobe University
Rokkodai, Nada, Kobe 657-8501, JAPAN

ABSTRACT

Flow visualization and particle image velocimetry (PIV) measurements were performed to reveal the three-dimensional structure of high frequency vortex shedding behind a V-gutter.

Tubular structures connecting adjacent vortices were found in front of the shedding vortex in the visualization image. PIV measurements permitted quantification of these tubular structures, although there were many errors in the results of these measurements. The overlap and moving average methods were applied to PIV-measured velocities to increase spatial resolution and to reduce errors. It was shown that the vortex shedding pattern behind a V-gutter forms into streamwise structures. The streamwise vorticity reached 20% to 100% of the spanwise vorticity at the same location. An FFT (Fast Fourier Transform) analysis was performed using the PIV data to determine the streamwise vorticity scale. This resulted in a calculated vortex diameter of 5mm, and this was verified by measurements taken from the visualization images.

INTRODUCTION

The bluff body type flame holder is commonly used in super/hypersonic aircraft engines (Lefebvre, 1998). The bluff body creates a recirculation zone and shear layer just behind itself, enhancing heat and mass transfer through turbulent diffusion (Mellor, 1990), and this recirculation zone has been investigated by many researchers (Hottel, et. al., 1962, and Davis and Bear, 1968). The present study investigates the wake of a bluff body flame holder, to determine how the flame holding mechanism is affected by the recirculation zone, and how the mixing characteristics are affected by vortex shedding from the recirculation zone (Hosokawa, et al., 1992, and Hosokawa, et al., 1994). We performed time-series velocity measurements using a fiber optic Laser Doppler Velocimeter (FLDV) (Hosokawa, et al., 1994). We found the relationships of the recirculation zone's length, strength and bulk velocity, using a circular type of bluff body (Hosokawa, et al., 1996). Secondly, we found that the vortices were shed from the coherent structure. FLDV data from time-series signals provided information about the turbulent structure of the flow behind the bluff body. Since FLDV is a point measurement technique, the results of this measurement provided temporal rather than spatial variations in the flow. If spatial information on the vortex and turbulence is desired, planar measurements are necessary.

When an obstruction such as a circular cylinder is placed in a flow, it produces vortex shedding. At low Reynolds numbers, this phenomenon is called Karman vortex shedding, and it is usually studied using flow visualization techniques (Tritton, 1970), (Hussain, 1980). Williamson et al. (1988) found streamwise vortices in flows with Re>180 in the Karman vortex phenomenon, but few have studied these streamwise vortices. Most experimental studies have examined only the laminar flows over these obstructions, and no one has investigated the streamwise vortex structure in highly turbulent flows over bluff bodies. The present study is an effort to perform such a study of the streamwise vortex shedding produced by bluff bodies in highly turbulent conditions ($Re=3.32x10^4$).

Vortex shedding causes the recirculation zone to oscillate, and this oscillation profoundly affects the air/fuel transfer and mixing. Previously, the vortex shedding at high Reynolds numbers could not be visualized clearly, because of a lack of temporal resolution, but recent developments in laser techniques have improved the spatial and temporal resolution of planar measurements to the point that visualization of high speed flows is now possible (Ikeda, et al., 1998), (Saito, et al., 1999).

The purpose of this experimental research is to investigate the three-dimensional structure of vortex shedding by using planar visualization, and estimate its dimensions using particle image velocimetry (PIV) measurements.

It seems that the formation of three-dimensional structures behind a bluff body is caused by a relationship between the upstream two-dimensional flow and the downstream three-dimensional turbulence.

EXPERIMENTAL CONDITIONS AND APPARATUS

Fig. 1 shows a schematic layout of the V-gutter test section, together with the digital particle image velocimetry (PIV) system. The main airflow was controlled at a bulk velocity between 40m/s and 100m/s, representing a Reynolds number of 3.32×10^4 to 8.29×10^4. Scattering particles (Nishigaki, et. al., 1992) were added to the upstream, and blown into the test section. The test section was 85mm square and 300mm long. The V-gutter was set 80mm downstream of the test section inlet. Optical windows were installed on each of the four sides for visualization and to measure the velocity by PIV. The cross-sectional shape of the V-gutter was pentagonal, with a wedge angle of 60 degrees, a side length of 15mm and 13.6mm square section. Air, in place of fuel, was supplied to the test section by jet holes 2.7mm in diameter set at 6.8mm pitch. The blockage ratio was 17.6%.

A Nd: YAG laser (max. 400mJ per pulse) was used as the illuminating source, and a high resolution CCD camera (1Kx1K) was used, in interlaced mode, to obtain single exposure double-frame images for cross-correlation processing. This cross-correlated image was then used to provide quantitative velocity data in PIV data processing. The measurement and processing parameters are shown in Tables 1 and 2.

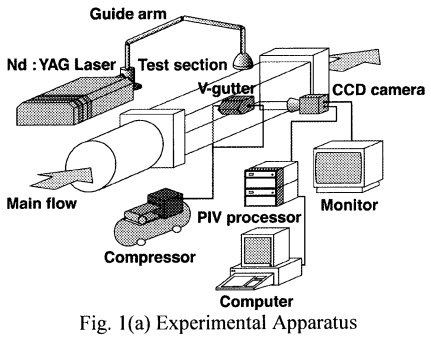

Fig. 1(a) Experimental Apparatus

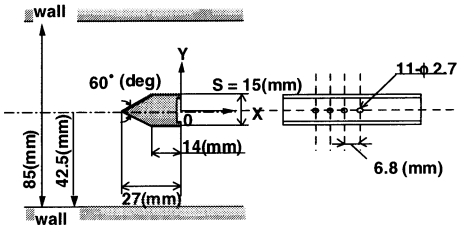

Fig. 1(b) V-gutter Configuration

Table 1 Optical Parameters

Laser	Spectra Physics PIV-400 Nd: YAG Pulse separation time Max. energy OSC/AMP Applied energy OSC/AMP	532nm, 10Hz 2, 3, 5 μsec 530 / 530 mJ 61.0 / 59.9 mJ
Laser Guide Arm	DANTEC 80x10 Optical tr. efficiency OSC/AMP	75.5 / 75.5 %
Sheet Froming Optics	DANTEC 80x20 Laser sheet thickness	0.8 - 1 mm
Camera	DANTEC Double Image 700 Number of active CCD pixels Scale factor	H = 768 (8906.1mm) V = 484 (6561.8mm) 6.634 56.69 x 41.85 mm
Lens	Nikon AF Micro Nikkor 60 1:2 8D Focal length Applied aperture	50 mm F4

RESULTS AND DISCUSSIONS

Visualization of vortex shedding

Flow visualization using a Nd: YAG laser-sheet was used to study the flow field behind the V-gutter. The seeding particles (Micro Spherical Feather) (Nishigaki, et. al., 1992) were fed into the upstream bulk flow. Fig. 2 shows a single image of the experimental flow field taken at a bulk velocity of 40 to 100m/s ($Re=3.32 \times 10^4$ to 8.29×10^4). Each pixel in the CCD array corresponded to an area 0.78mm x 0.84mm in physical size. The particle number density and particle diameter distributions produce a particular brightness level for each pixel. In the case of Micro Spherical Feather seeding, the particle diameter distribution is very narrow (2.7m in mean diameter +-1m range) (Nishigaki, et. al., 1992), so that the light intensity in the pixel depends only on the particle number density. The problem with this method is the inhomogeneous number density that is caused by particle followability.

The followability of a particle for coherent structures can be evaluated using the Stokes number S_t. This number represents the ratio of the recirculation response time τ_p of the particle to the characteristic time of the flow τ_f (Crowe, et. al., 1988, and Wen, et. al., 1992).

$$St = \frac{\tau_p}{\tau_f}$$

where

$$\tau_p = \frac{\rho_p d_p^{\,2}}{18 \mu_f}$$

ρ_p: particle density
d_p: particle diameter
μ_f: kinetic viscosity of the flow

For the present study, the characteristic flow time was taken as the reciprocal of the oscillating frequency as indicated by the time-series LDV data. Our previous report showed that the oscillating frequency of the flow was about 2kHz at a bulk velocity of 100m/s. This corresponds to a Stokes number of 8.79×10^{-3}, showing that the particles closely followed the flow.

The blockage ratio of the test section was 17.6%. This means that the air of 17.6% of the total cross sectional area of the test section was pressed behind the V-gutter. On the other hand, the reverse flow rate from the recirculating flow was estimated to be less than 5% that of the bulk airflow. As a result, the vortex structures were visualized as the shadow of Mie scattering in the images.

The black areas in this image represent the vortices. Consecutive vortex shedding behind the V-gutter, and vortex formation and evolution leading to enlargement can clearly be observed. This did not differ from at any

Table 2 PIV Parameters

Bulk velocity	40 m/s	60 m/s	80 m/s	100 m/s
Pulse sep. time	5 μsec	5 μsec	3, 5 μsec	2 μsec
Interr. Area (pixel)	16 x 16	32 x 32		64 x 64
Sptial resol. (mm)	1.16 x 1.34	2.35 x 2.73		4.71 x 5.50
Overlap	50 %	50 %		75 %
Int. Area Shift	4H pixels	4H pixels		4H pixels
No. of vectors / No. Shift	95 x 59 = 5605	47 x 29 = 1363		45 x 27 = 1215
vectors / 4H pixels Sh.	94 x 59 = 5546	46 x 29 = 1334		44 x 27 = 1188
Pulse sep. time	2 msec	3 msec		5 msec
Velocity equiv. with 4H pixel shift	139.1 m/s	92.7 m/s		55.6 m/s
Bulk velocity	40 m/s	60 m/s	80 m/s	100 m/s
Peak Valid. (S/N)	1.2			
Range Valid. Limit	50 m/s	90 m/s	100 m/s	170 m/s
Mov. Av. Validation	Aver. area: 3 x 3; Acceptance limit: 10 %			

velocity in the bulk velocity range examined (40-100m/s), and means that the vortex shedding phenomenon is universal at these high Reynolds numbers.

Two flow fields were visualized parallel and perpendicular to the V-gutter axis, in two planes, as shown in Fig. 3. The spanwise vortices were generated from the recirculation zone as a tube. Some spanwise vortices looked like oblique shedding (shown in Fig. 3(b)), and a few did not follow the tube formation pattern (shown Fig. 3(c)). These images show that the vortices are distributed along the axis of the vortex.

Visualization of streamwise vortex

Returning to the image of Fig. 2 it can be seen that the spanwise vortices were shed from each side alternately

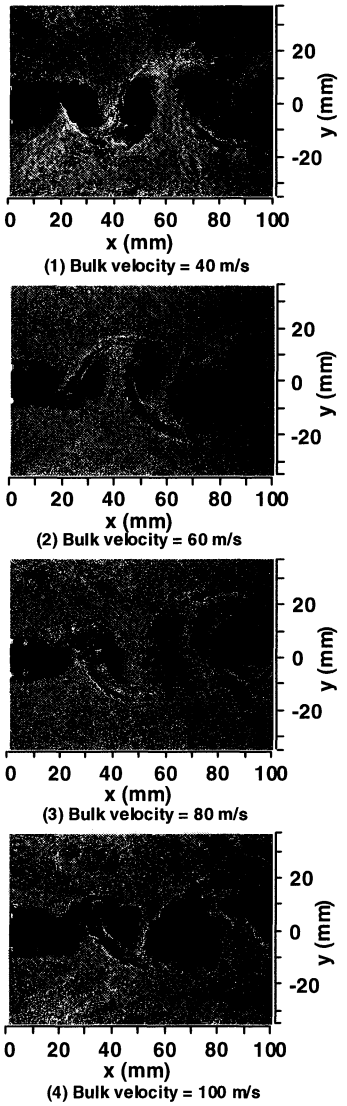

Fig. 2 Single Visualized Image of the Investigated Flow Field taken at a Bulk Velocity of 40 to 100m/s ($Re=3.32x10^4$ to $8.29x10^4$)

and that the vortices were connected together to form a "bridge". In earlier studies, examination of Karman vortex shedding focused only on the spanwise vortex, and few studies paid attention to other structures. Therefore, in order to verify the existence of this "bridge" structure, the visualized image at the top of the V-gutter was magnified, as shown in Fig. 4(a). This area was magnified to a size 30x30mm larger than in Fig. 3.

The black area on the right side of the visualization image shows the spanwise vortex attached to the V-gutter. This vortex is growing, and has not shed yet. There are alternating black and white areas in this image. Our interest is focused on the both sides of the black area. An obvious line is clearly visible at the downstream side of the vortex (black-white border), but at the upstream side of the vortex (white-black border), this borderline is very convoluted and appears to have circular shapes. The diameters of these circles were 3-5mm in the image. Fig. 4(b) shows the visualized area 20mm downstream from Fig. 4(a).

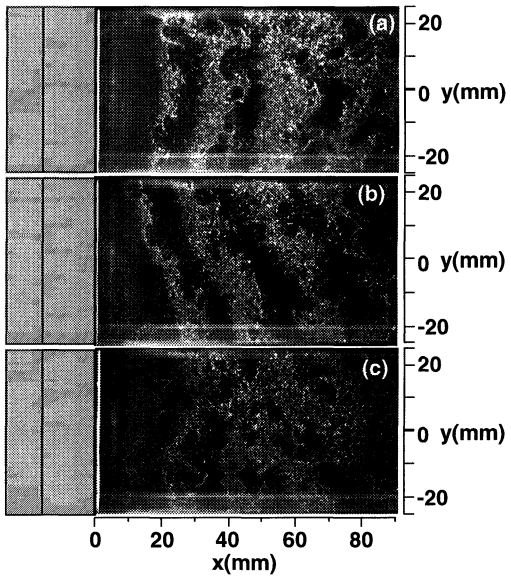

Fig. 3 Tubular Vortex Shedding Phenomena (Top View)

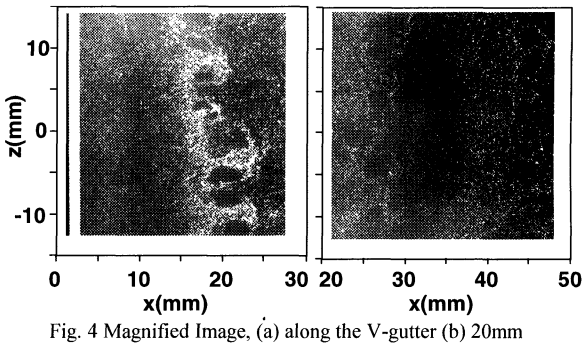

Fig. 4 Magnified Image, (a) along the V-gutter (b) 20mm downstream from V-gutter (Top View)

Many circles were seen in front of the black area. These circles were always on the upstream side of the spanwise vortex. This means that the circles might develop because of the interference between the high-speed primary flow and the upstream side of the low speed shedding vortex. The findings of this visualization are that the shedding vortices have a three-dimensional structure, rather than a two-dimensional structure.

Evaluation of post processing PIV measurements

In the previous section, it was shown that flow structures connected the tubular shedding vortices and that these structures formed in a row in front of the shedding vortex. We attempted to quantify the "bridge-like" structure using an understanding of the characteristics of "bridge-like" structures. If the "bridge-like" structure was the same as the streamwise vortex described by Williamson et. al. and Bernal and Roshko, then the direction of rotation of the streamwise vortices should have been reversed. PIV measurements were performed to quantify the "bridge-like" vortex structures.

Fig. 5 shows the ratio of error vectors to all vectors in the area measured by PIV, and the ratio of error vectors to vectors on a line across the "bridge-like" structure

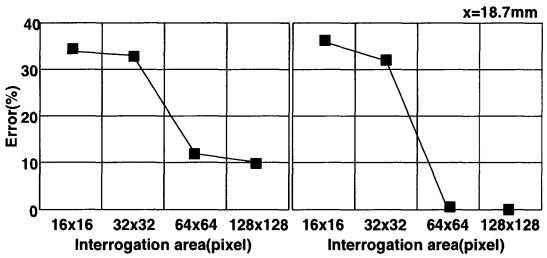

Fig. 5 Error Ratio in the whole Investigated Flow and on the cross line (x=18.7mm) (Top View)

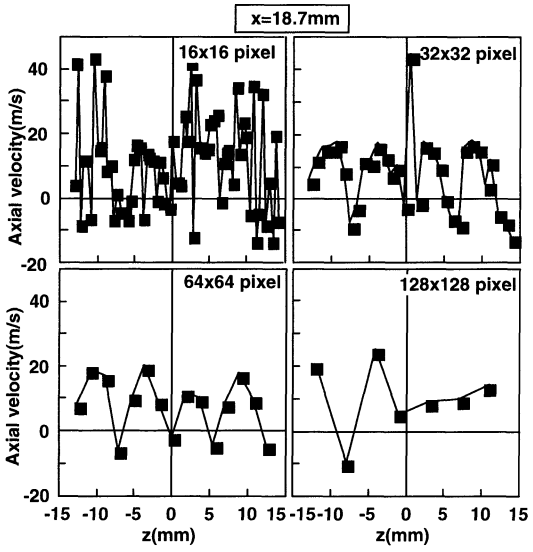

Fig. 6 Axial Velocity Distribution along the cross line (x=18.7mm) in the case of the each Interrogation Area

(x=18.7mm). Error vectors were decided following Peak Validation >1.2 by Adrian (1988). The size of the area interrogated changed: 16x16, 32x32, 64x64 and 128x128 pixels. The corresponding spatial resolutions were 0.446x0.446, 0.892x0.892, 1.784x1.784 and 3.568x3.568 mm, respectively. The error ratio differed from significantly between 32x32 and 64x64 pixels. An interrogation area larger than 64x64 pixels is essential to obtain a meaningful vector map from the visualization images, but the vector map included more than 10% error. The reason for these incorrect vectors was the cross sectional direction of the image obtained. The cross section of the visualized image was across the rotating vortex, so that the velocity through the measurement plane was high. Therefore, PIV measurement included many error vectors.

Next, the cross section across the circular structure (x=18.7mm) was examined. Fig. 6 shows the axial velocity distribution along this cross section for each size of interrogation area.

This graph indicates that the axial velocity had no strange values that caused errors. In the axial velocity distribution found using 16x16 pixels, no pattern could be obtained due to the large number of incorrect velocity vectors. But at 32x32 pixels, the pattern was the same as for 64x64 pixels, even though the error ratio differed. There were large errors in the velocity near the center of the z-axis at 32x32 pixels, and there was a resolution problem at 64x64 pixel for the circular structure analyzed.

In order to solve these problems, post-processing was examined. The overlap method was applied to increase the spatial resolution, and the moving average method was used to decrease the velocity errors. The overlap method increases the spatial resolution by superimposing interrogation areas.

Fig. 7(a) shows the axial velocity distribution, with a comparison of the different overlap ratios, 0% and 50%, analyzed at 32x32 pixels. Fig. 7(b) shows the same comparison with the size of the interrogation area increased to 64x64 pixels. The spatial resolution at 64x64pixels with an overlap ratio of 50% was the same as the resolution with 32x32 pixels and an overlap ratio of 0%.

As the overlap ratio increased as 32x32pixels, the number of error velocities increased due to the large errors inherent in measurements over such a small grid. At 64x64pixels, the flow pattern was not significantly changed with increasing spatial resolution, because the axial velocities had smaller errors.

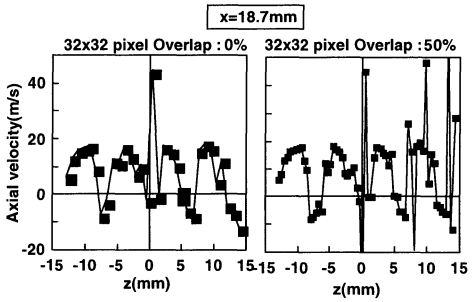

Fig. 7(a) Axial Velocity Distribution along the cross line (x=18.7mm), Interrogation Area =32x32pixels, Overlap 0% and 50%

Secondly, the moving average method was applied to the large velocity errors produced by the overlap method. The two-dimensional moving average method is expressed as follows (Host-Madsen and McCluskey, D. R., 1992):

$$v(x,y)=\frac{1}{mn}\sum_{i=x-\frac{m-1}{2}}^{x+\frac{m-1}{2}}\sum_{j=y-\frac{n-1}{2}}^{y+\frac{n-1}{2}}v(i,j)$$

Fig. 8 shows the axial velocity distribution after applying the moving average method. For comparison, the velocity distribution resulting from an overlap ratio of 50% at 64x64 pixels is also shown.

This diagram shows that the velocity distribution with 50% overlap at 32x32 pixels is almost the same as at 64x64 pixels. The mean and RMS velocities calculated from the velocity distributions for 50% overlap at 32x32 pixels and 50% overlap at 64x64 pixels were compared. The difference between the two was <5% for both the mean velocity and rms. The result of this analysis is that even if a vector map has many incorrect vectors, it is still possible to use this information if the image is focused and post-processed properly. Fig. 9 shows (a) a visualized image, (b) a vector map and (c) the corresponding vorticity distribution with an overlap ratio of 50% at 32x32 pixels.

In this paper, only the phenomena near x=20mm have been examined. This circular structure can be regarded as a structure of staggered pairs. The vector map and vorticity distributions show that the vortices rotate and spin. Previously, Bernal and Roshko (1988) discovered three-dimensional motion in the planar mixing layer. It was shown that a secondary streamwise structure is superimposed on the primary spanwise vortex structure.

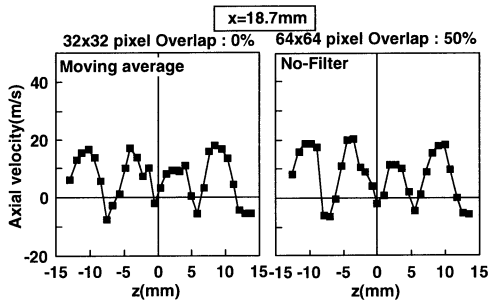

Fig. 7(b) Axial Velocity Distribution along the cross line (x=18.7mm), Interrogation Area =32x32pixels, Overlap 0% and 50%

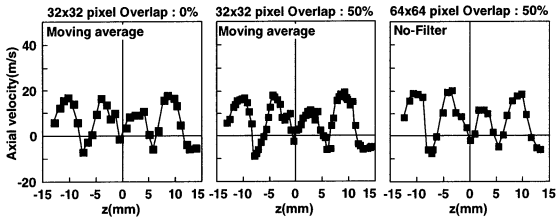

Fig. 8 Effect of Moving Average method to the Velocity Distribution

The streamwise structures were studied using point measurements and flow visualization. In this case, the circular structures were streamwise vortices similar to those in the mixing plane. It seems that the development of the streamwise vortices is due to the interference between the high speed shedding and the primary flow. It follows that the previously mentioned "bridge" structures were curling streamwise vortices.

Streamwise Vortices and Three-dimensional Structures

Fig. 10 shows the streamwise structures and their vorticity distribution in the axial direction.

The vorticity distribution varied widely. The streamwise vorticities reached 20% to 100% of the spanwise vorticities at the same locations. The streamwise vortices were very strong structures.

Next, the streamwise vortex scale was considered. The diameter of the streamwise vortex appeared to be about 3 to 5mm in the visualized images. If the vortex scale is determined by measurements from visualization images, the size varies with the characteristics of the seeding particles. Therefore, the vortex scale was determined from the vortex pitch as calculated by the application of FFT techniques. Fig. 11 shows the axial velocity power spectrum calculated from the data shown in Fig. 8. The horizontal axis indicates the inverse of the vortex scale. In this analysis, the size of the interrogation area was 32x32pixels, which corresponds to a spatial resolution of 0.446x0.446mm. This implies that vortex scales less than 0.446 mm were meaningless.

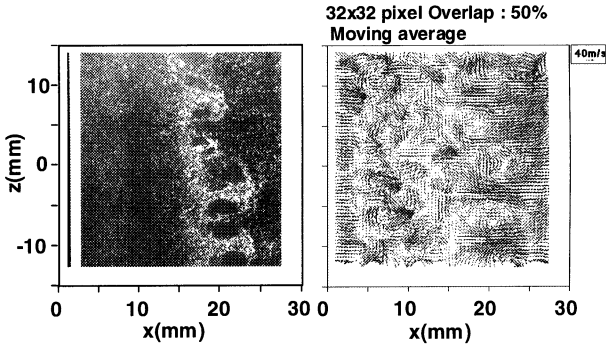

Fig. 9(a) Visualized Image Fig. 9(b) Vector Map

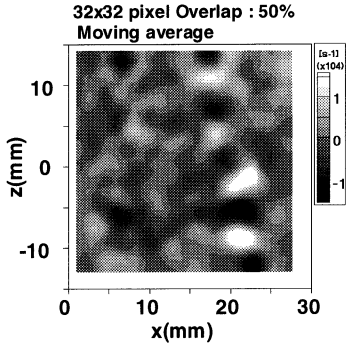

Fig. 9 (c) Vorticity Map (Interrogation Area=32x32pixels, Overlap 50%)

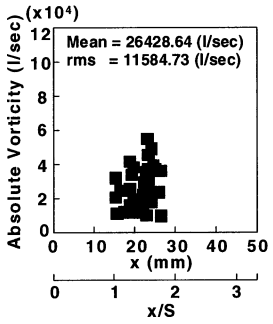

Fig. 10 Streamwise Vortices' Vorticity Distribution

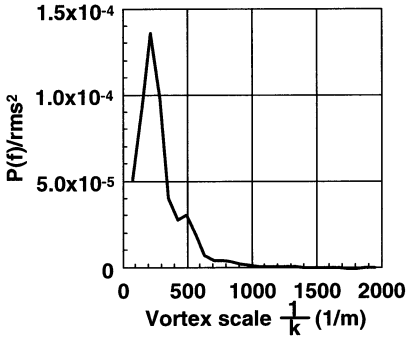

Fig. 11 Power Spectrum Distribution by FFT Analysis

The peak was dispersed because of the relatively small number of samples, but a peak could still be distinguished. This peak value was 0.208. The inverse of the peak was 4.81mm, and this agrees well with the vortex scale measured from the visualization image.

It is therefore clear that there are two kinds of vortices in the vortex shedding phenomenon in high-speed flows; spanwise vortices and streamwise vortices. As a result, the vortex shedding phenomenon must be considered to be three-dimensional.

Fig. 12 shows a model of the three-dimensional vortex shedding phenomenon in a high-speed flow.

CONCLUSIONS

Vortex shedding behind a V-gutter was visualized and measured by PIV to illustrate the three-dimensional structures. It was shown that the vortex shedding phenomenon behind a V-gutter has streamwise structures similar to those in a plane-mixing layer. The streamwise vorticities were 20% to 100% of the spanwise vorticities at the same locations. To determine the streamwise vortex scale, the axial velocity distribution obtained using PIV measurements was analyzed using FFT techniques. The streamwise vortex scale was found to be approximately 5mm and this is confirmed by measurements taken from the visualization images.

REFERENCES

Lefebvre, A. H., 1998, "Gas Turbine Combustion",

Mellor, A. M., 1990, "Design of Modern Turbine Combustor", ACADEMIC PRESS

Hottel, H. C., Williams, G. C., Jensen W. P., Tobey, A. C. and Burrage, M. R., 1962, "Modeling studies of Baffle-Type Combustor", 9th *symp. (Int.) on Comb.*, pp923-935

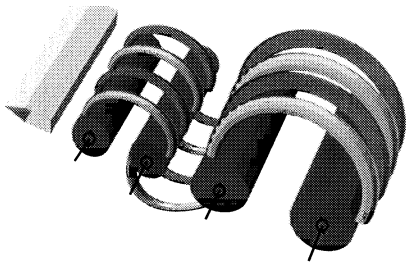

Fig. 12 Three-dimensional Structure Model behind V-gutter in High-Speed Flow

Davis, T. W. and Beer, J. M., 1968, "Flow in the wake of Bluff-Body Flame Stabilizers", *13th Symp. (Int.) on Comb.*, pp631-638

Hosokawa, S., Ikeda, Y. and Nakajima T., 1992, " Flow characteristics downsream of V-Gutter type Flame Holder in High Speed Flow", *6th Int. Symp. on Applics of Laser Tech. to Fluid Mech.*, pp19.3.1-19.3.8

Hosokawa, S., Ikeda, Y., Minato, M. and Nakajima, T., 1994, "Flow measurements behind V-gutter under Non-combusting Condition", *AIAA paper 93-0020*

Tritton, D. J., 1970, "Experiments on flow past a circular cylinder at low reynolds numbers", *J. Fluid Mech.*, Vol.6, part 4, pp547-567

Hussain, A. K. M. F., 1986, "Coherent structures and turbulence", *J. Fluid Mech.*, vol. 173, pp303-356

Williamson, C. H. K., 1988, "The existence of two stages in the transition to three-dimensionality of a cylinder wake", *Phys. Fluids* 31(11), pp3165-3168

Ikeda, Y., Saito, T., Rohaly, J., Kuratani, N. and Nakajima, T., 1998, "Quantitative Visualization of High Speed Vortex-Shedding Flow and Its Characteristics", *8th Int. Symp. on Flow Visualization*, pp280.1-280.8

Saito, T., Kuratani,N., Ikeda, Y. and Nakajima, T., 1999, "Visualization and PIV Measurement of Vortex Shedding behind V-shaped Gutter", *5th ASME/JSME Thermal Engineering Conference*, pp

Nishigaki, M., Ippommatsu, M., Ikeda, Y., Nakajima, T., "New High-Performance Tracer Particles for Optical Gas Flow Diagnostics", 1992, Measurement Science and Technology, Vol.3, p619-621

Crowe, C. T., Chung, J. N. and Troutt, T. R., 1988, "Particle mixing in free shear flows", *Pog. Energy Combust. Sci.*, Vol.14, pp171-194

Wen, F., Kamalu, Chung, J. N., Crowe, C. T. and Troutt, T. R., 1992, "Particle dispersion by vortex structures in plane mixing layers", *J. of Fluids eng.*, Vol.114, pp657-666

Janos, R., Nakajima, T., Ikeda, Y., "False Displacement Peak Based Improvement of Particle Image Velocimetry to Detect Flow Fields Exhibiting Large Velocity Gradients", 1999, 5th ASME/JSME Thermal Engineering Joint Conference

Adrian R.J., 1988, "Statistical properties of particle image velocimetry measurements in turbulent flow", *Laser Anemometry in Fluid Mechanics - III.*, pp. 115-129

Bernal, L. P. and Roshko, A., 1986, "Streamwise vortex structure in plane mixing layers", *J. Fluid Mech.*, vol.170, pp499-525

Host-Madsen, A. and McCluskey, D. R., 1992, "On the accuracy and reliability of PIV measurements", *7th Symp. (Int.) on Appli. of Laser Tech. to Fluid Mech.*, pp26.4.1-26.4.11